On the Models for the Investigation of Charged Defects in Solids: The Case of the VN- Defect in Diamond

On the models for the investigation of charged defects in solids. The case of the VN^- defect in diamond.

Roberto Dovesi,[*,†] Francesco Silvio Gentile,[‡] Anna Maria Ferrari,[‡] Fabien Pascale,[¶] Simone Salustro,[†] and Philippe D'Arco[§]

†*Dipartimento di Chimica, Università di Torino and NIS (Nanostructured Interfaces and Surfaces) Centre, Via P. Giuria 5, 10125 Torino, Italy*

‡*Dipartimento di Chimica, Università di Torino, Via P. Giuria 5, 10125 Torino, Italy*

¶*Theory-Modeling-Simulation group, SRSMC, CNRS, University of Lorraine, BP 70239, 54506, Vandoeuvre-les-Nancy, France*

§*Sorbonne Université, CNRS-INSU, Institut des Sciences de la Terre Paris, ISTeP UMR 7193, F-75005 Paris, France.*

E-mail: francesco.gentile@unina.it

April 3, 2019

Abstract

Local charged defects in periodic systems are usually investigated by adopting the *supercell charge compensated* (CC) model, that consists of two main ingredients: i) the periodic supercell, hopefully large enough to reduce to negligible values the interaction among defects belonging to different cells; ii) a background of uniform compensating charge that restores the neutrality of the supercell and then avoids the "Coulomb catastrophe". Here an alternative approach is proposed and compared to CC, the *double*

defect (DD) model, in which another point defect is introduced in the supercell, that provides (or accept) the electron to be transferred (subtracted) to the defect of interest. The DD model requires obviously a (much) larger supercell than CC, and the effect of the relative position of the two defects must be explored. A third possible option, the cluster approach, is not discussed here.

The two models have been compared with reference to the VN^- defect; for DD, the positive compensating charge is provided by a P atom. Three cubic supercells of increasing size (containing 216, 512 and 1000 atoms) and up to eight relative VN^- - P^+ defect-defect positions have been considered. The comparison extends to the equilibrium geometry around the defect, band structure, charge and spin distribution, IR and Raman vibrational spectra and EPR constants. It turns out that the CC and DD models provide very similar results for all these properties, in particular when the P^+ compensating defect is not too close to VN^-.

Introduction

Defects in solids play a fundamental role, as many of the properties of the pristine material can be altered by defects. Hence the need of eliminating defects, or, alternatively, of introducing in a controlled way specific defects. A large fraction of the local defects are classified as *charged*. In the literature, these defects are indicated as A^{n+} or B^{m-}, with m and n integers. This means that within a sphere of arbitrary but limited radius R (say 2-5 Å?) the sum of positive and negative charges is not equal to zero. The definition of the radius R, and the partition of the charge in the two regions, *inside* and *outside* the sphere, can obviously be matter of discussion.

The most common model adopted for describing local charged defects in periodic systems consists in two main ingredients: i) the supercell scheme (a multiple of the primitive cell of the perfect host system, large enough to reduce hopefully to negligible values the interaction

of defects belonging to different cells); ii) a background of uniform compensating charge that restores the neutrality of the supercell and then avoids the "Coulomb catastrophe".[1–4]

This model, to be indicated here as CC (*charge compensated*) is somehow innatural, as on the basis of simple electrostatic considerations, any (say) positively charged A^+ defect, must be compensated by a negatively charged B^- defect at a relatively short distance. Then the CC model implies that i) the background charge is not altering the properties of A^+, and ii) that in most of the cases the B^- defect, although close to A^+, is not such to alter significantly its properties.

An alternative scheme consists in introducing a second defect, of opposite charge, so that the supercell turns out to be neutral. One of the differences between the two models is that in the former (CC), a single spatial configuration exists (the compensating charge is not centered at a given point of the cell, being uniform), whereas in the latter the relative position of the two defects bearing the positive and negative charge must be explored. So in the DD case a space with many more variables than in CC must be considered. The DD model also requires larger supercells, because the B^- defect must be sufficieltly far from the A^+ defect and from all its images in neighboring cells. It is evident, however, that the DD approach is in principle more realistic than CC, and can be used to answer to the following question: *how the properties that are attributed to defect A^+ depend on the distance from (and orientation with respect to) a second defect B^-, and on the electronic structure of B^-?*

In the present paper we compare the CC and DD models with reference to various properties (geometry, charge and spin distribution, EPR constants, vibrational frequencies) of the so called VN^- defect in diamond (a vacancy with a nitrogen atom as first nearest neighbor and a negative charge floating around).

Despite the simplicity of the pristine lattice and the strength of the C-C bond, both natural and synthetic diamond contain, and are characterised by, a wide variety of point defects.[5–11] The investigation of the latter, both native and radiation-induced, has attracted strong experimental and theoretical interest. In particular the VN^- defect has been largely studied

for its peculiar properties suitable for technological applications (*qbit*).[12–14]

In the present study the atom that provides the compensating charge is (substitutional) P, that loses one electron that migrates then to the VN defect generating VN^-.

The structure of the paper is as follows: in the next section the models and the method are discussed. The results obtained with the CC and DD schemes are then presented. Some conclusions on the results obtained with the two models are finally drawn.

Computational Details

Method

All calculations have been performed by employing the *ab initio* CRYSTAL code,[15,16] the B3LYP "hybrid" functional[17,18] and a split valence 6-21G basis set[19] for the carbon and nitrogen atoms, except for values of 0.23 (C) and 0.30 (N) $Bohr^{-2}$ for the exponents of the outermost *sp* orbitals. This scheme is already well tested in previous works about diamond structures involving vacancy defects and nitrogen substitutions.[20–24] For the P atom a large core pseudopotential has been adopted so that only the five valence electrons are explicitly considered.[25] The truncation criteria of the Coulomb and exchange infinite lattice series are controlled by five thresholds, T_i, which have been set to 8 (T_1-T_4) and 16 (T_5). The convergence threshold on energy for the self-consistent-field (SCF) procedure has been set to 10^{-8} Ha for structural optimizations, and to 10^{-10} Ha for frequency calculations. The DFT exchange-correlation contribution and its gradient are evaluated by numerical integration over the unit cell volume. The generation of the integration grid is based on an atomic partition method, originally proposed by Becke,[26] in which the radial and angular points are obtained from Gauss-Legendre quadrature and Lebedev two-dimensional distributions respectively. In this study a pruned grid with 75 radial and 974 angular points has been used.

Vibrational spectra

Harmonic phonon frequencies, ω_p, at the Γ point (*i.e.* at the center of the first Brillouin zone in reciprocal space) are obtained from the diagonalization of the mass-weighted Hessian matrix of the second energy derivatives with respect to atomic displacements u:[27–31]

$$W^{\Gamma}_{a,i,b,j} = \frac{\mathcal{H}^{\mathbf{0}}_{a,i,b,j}}{\sqrt{M_a M_b}} \quad \text{with} \quad H^{\mathbf{0}}_{a,i,b,j} = \left(\frac{\partial^2 E}{\partial u^{\mathbf{0}}_{a,i} \partial u^{\mathbf{0}}_{b,j}} \right) , \tag{1}$$

where atoms a and b (with atomic masses M_a and M_b) in the reference cell, $\mathbf{0}$, are displaced by $u_{a,i}$ and $u_{b,j}$ with respect to the equilibrium geometry along the i-th and j-th Cartesian directions, respectively. Once the Hessian matrix, $\mathcal{H}^{\mathbf{0}}_{a,i,b,j}$, has been calculated, frequency shifts due to isotopic substitutions can be evaluated readily, at no computational cost, by changing masses in the above equation.

Energy first derivatives with respect to the atomic positions, $v_{a,i} = \partial E / \partial u^{\mathbf{0}}_{a,i}$, are calculated analytically for all coordinates, whereas second derivatives at $\vec{u} = \vec{0}$ are calculated numerically using a single displacement along each coordinate (the central point and a point to the right of the equilibrium position):

$$\left[\frac{\partial v_{a,i}}{\partial u^{\mathbf{0}}_{b,j}} \right] \approx \frac{v_{a,i}(0, \ldots, u^{\mathbf{0}}_{b,j}, \ldots)}{u^{\mathbf{0}}_{b,j}} \tag{2}$$

Previous calculations[27,32] have shown that in bulk systems the influence of u is very small (less than 1 cm^{-1}) when hydrogen atoms are not present.

Electron Paramagnetic Resonance

The coupling between the spin of the unpaired electron(s) ($\mathbf{S}$) and the system of the nuclear spins ($\mathbf{I}$) is described through the spin Hamiltonian:

$$H = \sum_n \mathbf{S} \cdot \mathcal{A}^n \cdot \mathbf{I}^n \tag{3}$$

where $\mathbf{I}^n$ and $\mathcal{A}^n$ refer to the nuclear spin and hyperfine coupling tensor related to the n^{th} nucleus, at site $\mathbf{R}_n$. $\mathcal{A}^n$ can be written in the form,

$$\mathcal{A}^n = A^n_{iso} \cdot I + \mathcal{B}^n \tag{4}$$

where I is a 3×3 identity matrix, or

$$A^n_{ij} = A^n_{iso}\delta_{ij} + B^n_{ij} \tag{5}$$

where A^n_{iso} is the isotropic contribution to $\mathcal{A}^n$, often referred to as the *Fermi contact term*, and $\mathcal{B}^n$ the anisotropic dipole-dipole interaction of the electron and nuclear spins. The Fermi contact term for an unpaired electron

$$A^n_{iso} = \frac{8\pi}{3} g_e \mu_e g_n \mu_N |\psi(\mathbf{R}_n)|^2 \tag{6}$$

relates to the direct interaction of nuclear and electron spins, and is only non-zero for states with finite electron spin density, $|\psi(\mathbf{R}_n)|^2$, at nuclear sites $\mathbf{R}_n$, namely those with unpaired electrons in s-subshells. g_e, μ_e, g_n and μ_N are the free-electron g-factor, Bohr magneton, gyromagnetic ratio of $\mathbf{I}^n$ and the nuclear magneton respectively.

The elements of the traceless tensor $\mathcal{B}^n$ at nucleus $\mathbf{R}_n$ are defined by:

$$B^n_{ij} = g_e \mu_e g_n \mu_N \int \mathrm{d}\mathbf{r}_n |\psi(\mathbf{r}_n)|^2 \Big(\frac{3\mathbf{r}_{ni}\mathbf{r}_{nj} - |\mathbf{r}_n|^2 \delta_{ij}}{|\mathbf{r}_n|^5} \Big) \tag{7}$$

where $\mathbf{r}_n$ is the distance to $\mathbf{R}_n$. $\mathcal{B}^n$ is usually written in terms of its three (principal axes) eigenvalues, B^n_1, B^n_2, B^n_3 and is a measure of the unpaired electron populations of valence p and d orbitals centered on the magnetic nucleus, and of all orbitals centered on neighboring atoms. Clearly $A^n_{iso} = \frac{A^n_1 + A^n_2 + A^n_3}{3}$, since $\mathcal{B}^n$ is traceless, and, for a nuclear site with axial symmetry, we have $A^n_{iso} = \frac{A^n_{\parallel} + 2A^n_{\perp}}{3}$ and $B^n_{\parallel} + 2B^n_{\perp}$=0.

Models

The long-established supercell approach is used to simulate different defect concentrations. Here cells containing 216, 512 and 1000 atoms have been considered, and indicated as S_{216} and S_{512} and S_{1000} in the following. Reciprocal space sampling is based on a regular Pack-Monkhorst[33] sub-lattice grid centered at the Γ point (*i.e.* at the center of the first Brillouin zone), leading to 2 (S_{216} and S_{512}) and 1 (S_{1000}) sampling points along each of the reciprocal lattice vectors, which correspond to 4 and 1 **k**-points in the irreducible part of the Brillouin zone respectively, after point symmetry has been taken into account.

Many results are summarized in Figure 1, that consists of 4 panels, each labeled from A to D. Panels A, B and C report the NV^- defect in the conventional cell of diamond, the local geometries, charge and spin distributions, and bond population of N, P and their neighbors, respectively. In panel D a schematic section view of the three supercells here considered is reported, where the position of the vacancy V (open square), of the nitrogen atom N (in blue) and of various locations of the P atom (in black) are shown. The N-V distance is 1.71$\pm$ 0.02 Å for the various P positions and cell sizes. In all cases the P atom is along the diagonal of the cubic supercell (actually pseudocubic: the C_{3v} symmetry of the high spin solution, S_z=1, entails a possible deformation of the cubic cell, that however remains totally negligible: the deviation of angles from 90° is as small as 0.2°, and the difference between the sides of the box is as small as 10^{-4} Å). The distances indicated on the figure are blue (red) when the P atom is closer to (farther from) the N atom and they correspond to S_{512}. In S_{216}, c and d are farther from the N atom (and then would be red); in S_{1000}, d is closer to and e, f, g, and h farther from the N atom. In the S_{216} and S_{1000} cases, distances deviate from the ones shown in the figure by no more than 0.01 Å.

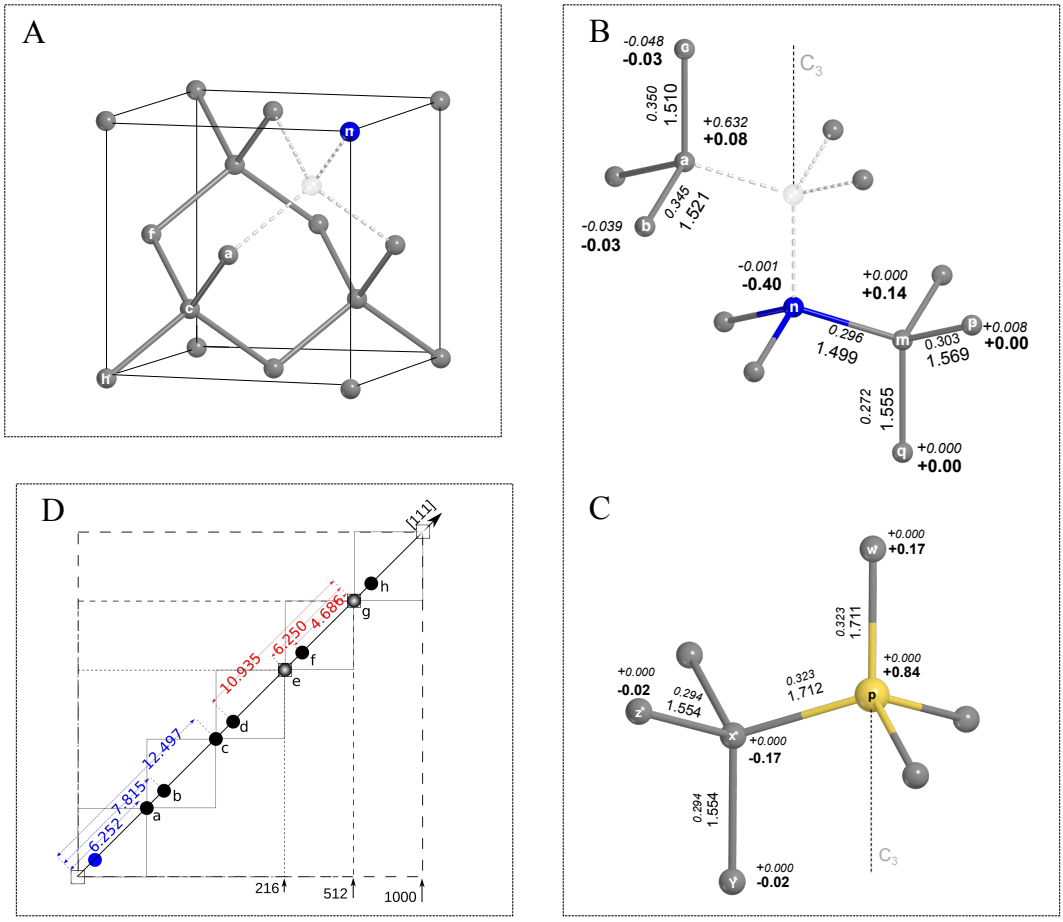

Figure 1: The NV^- point defect in the diamond conventional cell (A). Panels B) and C) show the local environment of NV^- and P^+, respectively. Distances (in Å), Mulliken net charges and spin momenta (in $|e|$, **bold** and *italic* respectively) and bond populations ($|e|$ and *italic*). Data refer to the NV^- defect in its triplet (S_z=1) state in S_{216} within the CC (charge compensated) scheme (B) and to the P neighborhood within the DD scheme (C). (D) is a sketch of the various positions of phosphorus (solid black circle) along the [111] direction in the supercell. The open square and the blue solid circle (bottom left) represent the vacancy and the nitrogen atom, respectively. 216, 512 and 1000 indicate the supercells used in this work; The small thin solid line squares outline the conventional cell of diamond. See text for more details.

Results

The compensating P^+ defect in the DD scheme.

Before starting the analysis of the local structure around the compensating P^+ ion, it is important to point out that, since its role here is to simply provide an extra electron to the lattice, in order to preserve the maximum number of point symmetry operators, it lies along the [111] direction in all the cases here presented. This choice leads to have 3 of the 4 first nearest neighbors of the P^+ ion to be symmetry related, being the fourth along the C_3 axis. From now on, only one value for each of the two sets will be reported. Note however that, in spite of the C_{3v} symmetry, the PC_4 tetrahedron is almost perfect, and the four charges of the C atoms are extremely similar. In Table 1 the Mulliken charges of the P atom and of its first and second neighbors as a function of the distance from the vacancy V and for the S_{1000} supercell are shown. The P net charge is about $+0.84|e|$ (q_P column); the net charge of each of its first neighbors is -0.17 $|e|$, to give a total of -0.68 $|e|$. The twelve second nearest neighbors further screen the charge of the P atom, as the last and second to last columns show. Overall the PC_{16} cluster (with a radius of 2.60 Å) is nearly neutral, with a net charge varying from $+0.005$ to -0.021 $|e|$ according to the V-P distance. In summary, when sufficiently far away from the VN defect, the P^+ defect is fully screened within a sphere of radius equal to 2.6 Å, and provides one electron to the VN defect to give VN^-.
The data for the S_{216} and S_{512} supercells, reported in Table S1 and Table S2 of the Supplementary Material section, are very similar to the ones just discussed.

Charge and spin density and the equilibrium geometry of the VN^- defect.

We consider now the VN^- defect, comparing the results of the CC scheme (last line in Table 2) with the ones of the DD scheme with different V-P distances.

We recall that the VN^0 (neutral) system has three uncoupled electrons on three carbon

Table 1: Relevant data concerning the neighborhood of the P atom within the DD model, as a function of the P position in the S_{1000} supercell (see Figure 1-D). R is the distance (in Å) between the vacancy V and the P atom, q (in $|e|$) are Mulliken charges. In the last column, the sum of the charges of the first and second neighbors of P are reported (it corresponds to the sum of the values shown in the three previous columns). For cases 1-4, N is in between V and P; in the other cases V is between N and P.

		R (Å)	q_P	q_{C_P}	$q_{C_P}(3)$	$\sum_1^{12} q_{C_P^2}$	$\sum_{C_P^1}^{C_P^2}$
a	V-N...P	6.252	+.843	-.170	-.170	-.158	-.838
b	V-N...P	7.818	+.841	-.168	-.170	-.192	-.870
c	V-N...P	12.490	+.841	-.170	-.170	-.180	-.860
d	V-N...P	14.050	+.841	-.170	-.170	-.183	-.863
e	V...P	12.492	+.841	-.170	-.170	-.183	-.863
f	V...P	10.931	+.841	-.170	-.170	-.180	-.860
g	V...P	6.260	+.840	-.167	-.170	-.192	-.869
h	V...P	4.693	+.843	-.169	-.173	-.156	-.844

Table 2: Mulliken charges q (in $|e|$) on atoms and distances R (in Å) between atoms or vacancy and atoms in the neighborhood of the VN defect for the various P positions in the S_{1000} supercell within the DD scheme. C_N indicates the three carbon atoms first neighbors of the nitrogen atom, C_V the three carbon atoms around the vacancy. The data in the last line refer to the charge compensated (CC) model.

	q_N	R_{C_N}	$q_{C_N}(3)$	R_{C_V}	$q_{C_V}(3)$
DD-a	-.393	1.499	+.140	1.509-1.520	+.075
DD-b	-.393	1.499	+.139	1.508-1.520	+.076
DD-c	-.394	1.499	+.138	1.509-1.519	+.077
DD-d	-.394	1.499	+.138	1.509-1.519	+.077
DD-e	-.394	1.499	+.138	1.508-1.519	+.078
DD-f	-.395	1.499	+.138	1.508-1.519	+.078
DD-g	-.395	1.500	+.137	1.505-1.519	+.079
DD-h	-.396	1.501	+.137	1.506-1.519	+.079
CC	-.395	1.499	+.137	1.509-1.520	+.076

atoms around the vacancy; the additional electron (coming from the P^+ defect, or simply *added* to the unit cell) would permit to generate a quintuplet (S_z=2, four electrons with α spin), a triplet (S_z=1, three α and one β electron) and a singlet (S_z=0, two α and two β electrons). The comparison between the CC or DD schemes refers to the triplet state. The Mulliken charges of the four atoms around the vacancy ($q_{C_V}(3)$ and q_N) and of the first neighbors of the latter ($q_{C_N}(3)$) are reported.

The table shows that in all the DD cases the net charges q and the equilibrium distances R are very similar among them, also in the cases in which the V–P (6.25 Å) or the N–P (4.69 Å) distances are relatively short. More interestingly, the CC and DD equilibrium distances and net charges essentially coincide, the largest difference being 0.003 $|e|$, and 0.003 Å.

We can then conclude that the CC model and the DD model in all its variants produce essentially the same local geometry and charge distribution.

The magnetic momenta μ, as obtained with the CC and DD models, and with supercells containing 216, 512 and 1000 atoms are shown in Table 3.

Table 3: Atomic magnetic momenta μ ($|e|$), evaluated according to a Mulliken partition of the spin density, for the CC and DD models. The labels following DD are the ones defined in Figure 1-D. Labels a, b, c, h of carbon atoms are defined in figure 1-A,B,C. Atom g, is a first neighbor of atom b in these figures. Numbers in parentheses indicate the multiplicity of the atoms. S stands for supercell.

	S	N	C_a (3)	C_c(3),	C_b(6)	C_g(6)	C_h(3)	P
CC	216	-0.001	0.632	-0.048	-0.039	0.038	0.034	0.000
CC	512	-0.001	0.632	-0.048	-0.039	0.038	0.034	0.000
DD-b	216	-0.001	0.632	-0.048	-0.039	0.038	0.034	0.000
DD-c	512	-0.001	0.631	-0.048	-0.039	0.038	0.034	0.000
DD-d	512	-0.001	0.631	-0.049	-0.039	0.038	0.035	0.000
DD-c	1000	-0.001	0.631	-0.049	-0.039	0.038	0.035	0.000
DD-d	1000	-0.001	0.631	-0.049	-0.039	0.038	0.035	0.000
DD-e	1000	-0.001	0.632	-0.048	-0.039	0.038	0.035	0.000
DD-f	1000	-0.001	0.632	-0.048	-0.039	0.038	0.035	0.000

As usual, for the DD model various distances are possible between the vacancy V and the P compensating cation. The spin momenta of the atoms labeled in Figure 1 are shown,

with their multiplicity. We remind that also relatively small spin momenta can provide visible contributions to the EPR spectrum. The table shows that the CC and DD results are very similar whichever the supercell is, the largest difference being always as small as 0.001 $|e|$. The same comment applies to the difference between the various supercells, and to the various positions of the P atom in the DD model. In summary, also such a delicate quantity as the magnetic momenta obtained with the CC and DD models essentially coincide.

The EPR constants.

The atomic magnetic momentum μ is an integrated quantity, that might miss local specific features of the spin density. We consider now the EPR parameters A_{iso}, the so called Fermi contact, that is the spin density at the position of the nucleus, and the three eigenvalues of the traceless symmetric hyperfine coupling tensor B (see equations 6 and 7). The comparison of the results of the CC and DD results are shown in Table 4. The values obtained with the CC and DD schemes are also for these properties very similar, and the difference is never larger than 1%.

The band structure.

In Figure 2 the band structure produced by the two models, CC and DD, when the S_{216} (top) and S_{512} (bottom) supercells are used, is reported. The most interesting eigenvalues, identified with numbers and open and full circles in Figure 2, are also reported in Table 5.

The figure shows that the CC and DD band structures are very similar, in particular in the valence and gap region (the occupied P levels fall down deep inside the valence band). This is not the case for the empty P^+ levels, that appear slighly below the conduction band. The *perfect bulk* gap is 5.80 eV. Here the difference between the valence and conduction manifolds is 5.89 eV large in CC, and reduces to 5.81 in DD for the S_{216} supercell. It

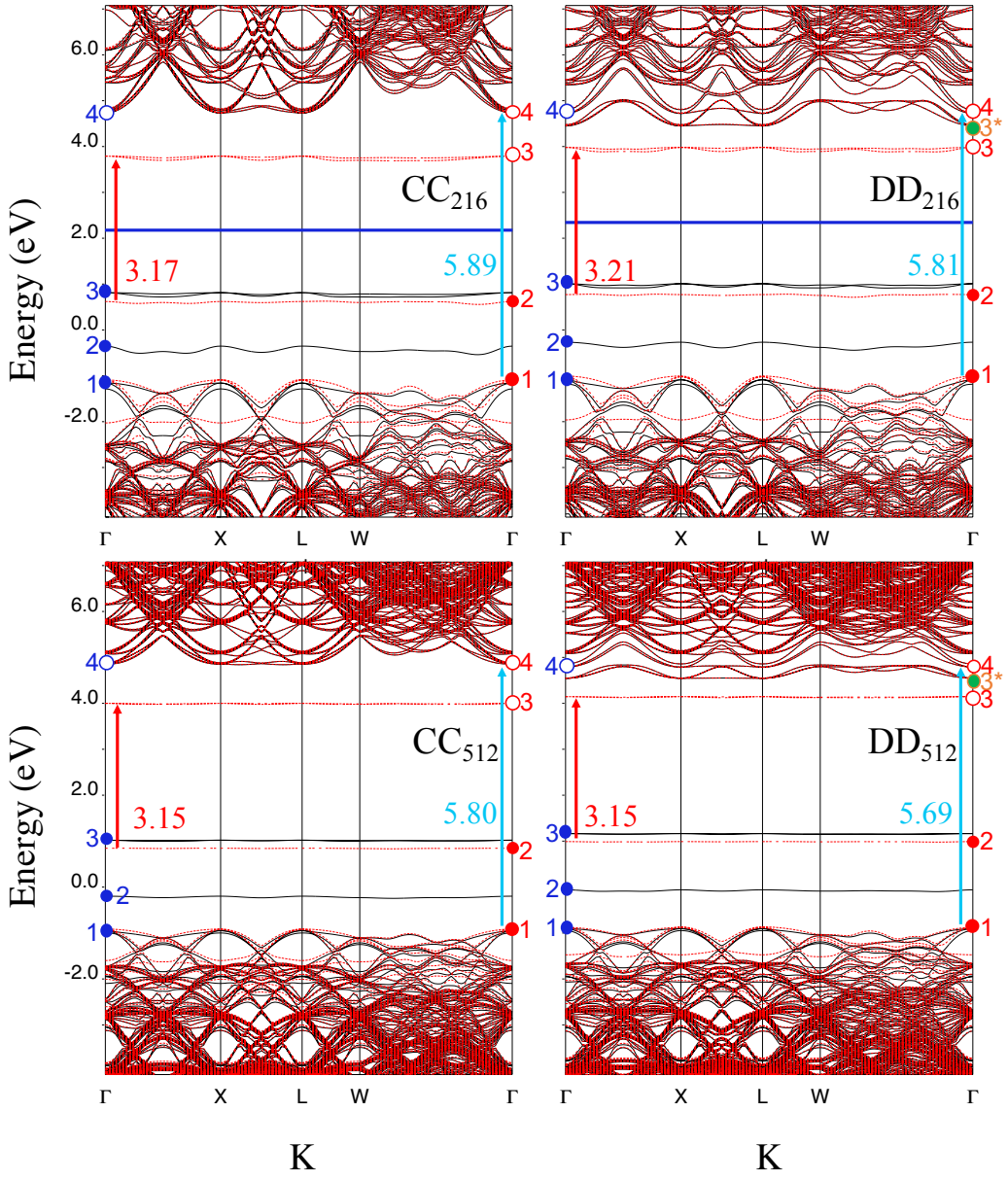

Figure 2: Band structure of the NV^- defect in its triplet (S_z=1) state, computed with the CC and DD models for the S_{216} and S_{512} supercells. The distance of the P^+ cation from the vacancy is 12.497 Å in S_{512}, and corresponds to the c position. The distance in S_{216} is 7.815 Å corresponding to the b position (see figure 1-D). The red arrows represent the direct band gap of the hosting defective level (donor band of the nitrogen center). The turquoise arrows indicate the gap of the hosting diamond. Gaps are evaluated in Γ and reported in eV.

Table 4: Hyperfine coupling constants (in MHz) of the NV^- defect in its triplet fundamental state as described by the CC (charge compensated) and DD (P^+ compensated) models. All calculations performed at the B3LYP/6-21G level. The labels of the two carbon atoms as in Table 3. S stands for supercell.

site	model	S	A_{iso}	B_1	B_2	B_3
^{14}N	CC	216	-2.14	-0.18	-0.18	0.35
	DD	216	-2.14	-0.18	-0.18	0.35
	CC	512	-2.15	-0.18	-0.18	0.36
	DD	512	-2.20	-0.18	-0.18	0.36
	DD	512	-2.10	-0.18	-0.18	0.36
	DD-c	1000	-2.05	-0.18	-0.18	0.36
	DD-d	1000	-2.11	-0.18	-0.18	0.36
	DD-e	1000	-2.15	-0.18	-0.18	0.36
	DD-f	1000	-2.16	-0.18	-0.18	0.36
$^{13}C_a$	CC	216	178.29	-22.32	-22.03	44.35
	DD	216	178.06	-22.32	-22.03	44.35
	CC	512	178.94	-22.31	-22.01	44.32
	DD	512	179.13	-22.29	-22.00	44.29
	DD	512	178.67	-22.29	-21.98	44.27
	DD-c	1000	179.01	-22.32	-22.00	44.32
	DD-d	1000	178.78	-22.29	-21.99	44.28
	DD-e	1000	179.22	-22.32	-22.01	44.33
	DD-f	1000	179.17	-22.31	-22.01	44.32
$^{13}C_g$	CC	216	18.17	-1.56	-1.39	2.94
	DD	216	18.31	-1.54	-1.37	2.91
	CC	512	18.24	-1.59	-1.37	2.96
	DD	512	18.21	-1.58	-1.37	2.95
	DD	512	18.15	-1.59	-1.38	2.96
	DD-c	1000	18.32	-1.59	-1.37	2.96
	DD-d	1000	18.11	-1.60	-1.37	2.97
	DD-e	1000	18.31	-1.59	-1.37	2.96
	DD-f	1000	18.32	-1.59	-1.37	2.96

Table 5: Electronic levels obtained with the CC and DD models and the S_{216} and S_{512} supercells. The numbers in the first column (where also the $1s$ α and β levels of nitrogen are shown) refer to figure 2. In the second column the occupancy of the levels is indicated: 1 for occupied and 0 for virtual levels. δ is the energy difference between the CC and DD values. The 3_1^* and 3_2^* lines report P levels, and do not appear then in the CC case. The largest absolute δ value of each column is in bold. Energy in Ha.

			$\mathbf{S}_{216}$			$\mathbf{S}_{512}$		
		OC.	CC	DD	δ	CC	DD	δ
α	1s(N)	1	-14.2080	-14.2060	-0.0020	-14.1990	-14.1930	**-0.0060**
	1	1	-0.0426(2)	-0.0399(2)	-0.0027	-0.0349(2)	-0.0333(2)	-0.0016
	2	1	-0.0129	-0.0098	-0.0031	-0.0073	-0.0022	-0.0051
	3	1	0.0299(2)	0.0370(2)	**-0.0071**	0.0375(2)	0.0428(2)	-0.0053
	3_1^*	0	–	0.1635(2)		–	0.1670(2)	
	3_2^*	0	–	0.1644		–	0.1672	
	4	0	0.1738(2)	0.1735(2)	0.0003	0.1784(2)	0.1760(2)	0.0024
β	1s(N)	1	-14.2080	-14.2060	-0.0020	-14.1990	-14.1930	**-0.0060**
	1	1	-0.0397	-0.0369	-0.0028	-0.0335	-0.0317	-0.0018
	2	0	0.0228	0.0283	-0.0055	0.0311	0.0364	-0.0053
	3	0	0.1393(2)	0.1463(2)	**-0.0070**	0.1470(2)	0.1523(2)	-0.0053
	3_1^*	0	–	0.1638(2)		–	0.1670(2)	
	3_2^*	0	–	0.1647		–	0.1672	
	4	0	0.1740(2)	0.1738(2)	0.0002	0.1785	0.1760(2)	0.0025

decreases to 5.80 eV for CC, and 5.69 eV for DD in the S_{512} cell. The CC - DD difference is then 0.08 eV and 0.011 eV for the smaller and larger supercells, indicating (as the analysis of the eigenvectors confirms) that in what we call the *perfect diamond* conduction band there is still some P^+ contribution.

We remind that the eigenvalues are defined with respect to a zero level that in the CRYSTAL code is the mean value of the potential in the unit cell. In order to appreciate how this zero reference changes from CC to DD, let us consider the $1s$ nitrogen eigenvalues shown in Table 5. The difference is as small as 2 mHa for the α electrons, and 6 mHa for the β.

This underlines that the different number of valence α and β electrons has some influence also on the deep levels as nitrogen $1s$. The difference between CC and DD remains constant in going from S_{216} to S_{512}. Both Figure 2 and Table 5 show that not only the order in energy of the defect levels (both α and β and occupied and virtual) is the same, but also that the numerical values are very similar with a maximum difference equal to -0.007 Ha (0.2 eV).

In summary, the two models produce quite similar band structures, if the levels of the *other* (P^+) defect are local, identified and then excluded from the comparison.

The vibrational spectrum.

In this section we will compare i) the vibrational frequencies and ii) the IR and Raman intensities produced by the CC and DD models; that is to say, we will compare the CC and DD IR and Raman spectra.

In Figure 3 the IR spectra of the VN^- defect obtained with the CC (top left) and DD (top right) schemes are reported. The DD spectrum obviously contains contributions from the P^+ defect, and then the comparison cannot be quantitative, but only qualitative. It is however possible to somehow *clean* the DD spectrum from the P related modes. To this aim the spectrum is also generated when the mass used for P in Equation 1 is four times (124 a.m.u: bottom left) or ten times (310 a.m.u: bottom right) larger of the 100% abundant isotope ^{31}P, and the dynamical matrix diagonalized again (this is obtained with the *ISOTOPES* option, see comment after Equation 1 in the methodological section). The VN^-P^+ spectrum presents a continuous band in the range 364-1332 cm^{-1} (S_{216}), with a few dominant peaks. Some of them are labeled in Figure 3 and in Table 6. The peaks of CC at wavenumbers higher than 600 cm^{-1} appear also in DD, and remain nearly unaltered when the P mass is four times or ten times larger than the one of most abundant isotope, the maximum difference being 8 cm^{-1}. There is also a peak at low wavenumbers (label 1 in Table 6) that appears both in CC and DD ^{31}P, and that remains nearly unaltered when the P mass is increased.

Other low wavenumber peaks, on the contrary, are quite sensitive to the P mass change; progressively, they shift down below 400 cm^{-1}. The IR intensities are only qualitatively similar. The comparison is in part biased by the fact that the spectrum is nearly a continuum of peaks (in the figures a Lorentzian convolution with a full width at half maximum, FWHM, of 8 cm^{-1} has been applied for mimic the experimental peak profile; indeed this choice leads to the *merge* in one broadened absorption band all the peaks that differ by a few cm^{-1}). In this situation the eigenvectors of contiguous eigenvalues are similar, and relatively important

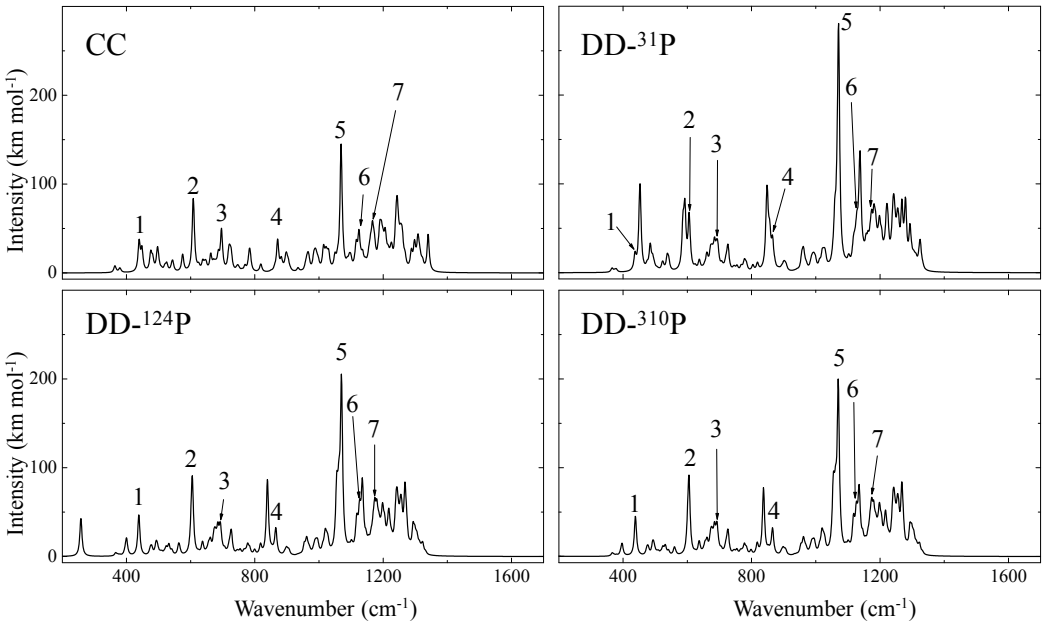

Figure 3: The IR spectrum of the VN^- defective diamond. Top panels: the charge compensated (CC) and P^+ compensated (DD - ^{31}P) results. Bottom panels: the DD scheme but multiplying the mass of phosphorus by 4 (DD - ^{124}P) and 10 (DD - ^{310}P), in order to *clean* the spectrum from peaks involving P, pushing them towards low wavenumbers. All spectra refer to S_{216} supercell. P is in position *b* of Figure 1-D.

mixing can be generated by small perturbations. In any case the Table confirms that these peaks not only appear in the two cases, but have relatively similar intensities.

As regards the Raman spectrum, the comparison between the CC and DD methods is simpler with respect to the IR one because the contributions of the normal modes involving mainly the P atom are relatively less intense.

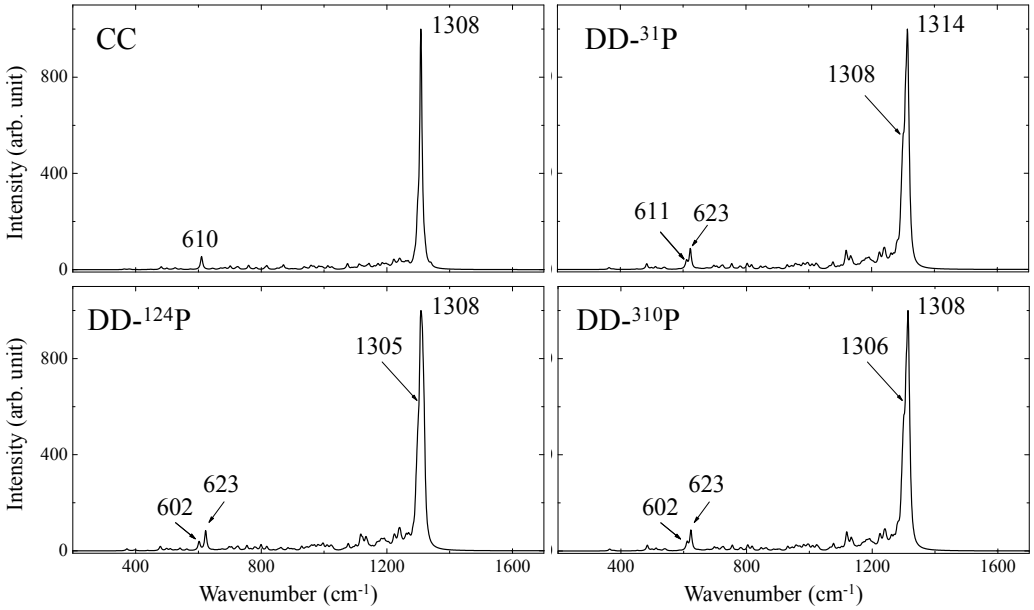

Figure 4: The Raman spectrum of the VN^- defective diamond using the S_{216} cell. Top panels: charge compensated (CC, left) and double defect (DD - ^{31}P, right) models. P is in position *b* of Figure 1-D. Bottom panels: DD scheme but multiplying the mass of phosphorus by 4 (DD - ^{124}P) and 10 (DD - ^{310}P), in order to *clean* the spectrum from peaks involving P, pushing them towards low wavenumbers.

The CC spectrum has a dominant peak at 1308 cm^{-1}, with a second peak at 610 cm^{-1}. To the left of the 1308 cm^{-1} peak there is a broad band, of low intensity, decreasing down to zero through a few minor peaks. In the ^{31}P spectrum the dominant peak is at 1314 cm^{-1}, with a shoulder at 1308 cm^{-1}. This peak shifts to 1308 in the ^{124}P and ^{310}P spectra. In the region of the CC 608 cm^{-1} peak, the ^{31}P spectrum shows two peaks at 611 and 623 cm^{-1}; the former shifts to 602 cm^{-1} in ^{124}P, with a decreased intensity. The latter remains at 623 cm^{-1}. The ^{310}P spectrum essentially coincides with the ^{124}P one. The broad low intensity

Table 6: Wavenumber (cm^{-1}), symmetry and intensity (km mol^{-1}) of seven intense peaks obtained with the CC model. The same peak data obtained with the DD model when the most abundant isotopic mass is used for phosphorus (DD-^{31}P), or the latter multiplied by four (DD-^{124}P) and ten (DD-^{310}P) are also shown.

	CC		**DD -^{31}P**		**DD -^{124}P**		**DD -^{310}P**	
N	$\tilde{\nu}$	I	$\tilde{\nu}$	I	$\tilde{\nu}$	I	$\tilde{\nu}$	I
1	439(E)	34	437(E)	18	438(E)	51	438(E)	49
2	608(E)	74	606(E)	61	605(E)	79	605(E)	80
3	696(E)	47	695(E)	21	693(E)	21	693(E)	21
4	871(E)	22	865(E)	28	865(E)	28	865(E)	28
5	1069(E)	145	1071(E)	278	1070(E)	202	1070(E)	197
6	1125(E)	38	1128(E)	27	1127(E)	31	1126(E)	28
7	1166(E)	27	1174(E)	37	1174(E)	37	1174(E)	37

band observed to the left of the 1308 cm^{-1} peak in CC, appear, with similar shape and slightly higher intensity, also in the DD cases.

In summary, the CC and DD Raman spectra are extremely similar.

The effect of the V-P distance on the spectra.

Since in the DD model the results may be affected by the mutual interaction between VN^- and P^+, in this section we explore the effect of the distance among the two defects, limiting however the analysis to the IR and Raman spectra, that are expected to be the most sensitive quantities. The mutual interaction increases as the size of the supercell decreases, so that all the results presented hereafter refer to S_{216}. Figure 5, left, compares the IR spectra of the VN^- P^+ defect in S_{216} when P^+ is occupying the four possible positions a, b, c, d along the diagonal. The vertical lines guide the eye in following the shift of some of the peaks. The distance of P from the center of the vacancy in the reference cell increases from 6.273 to 7.829 to 12.493 to 14.052 Å; the distance of P from N is 4.574 (a), 6.112 (b), 7.983 (c) and 6.403 Å (d). Using the (b) case as a reference, Figure 5 shows that the largest shifts for the various cases never exceeds 17 cm^{-1}.

Some peaks seem to be much higher for some P distances than for others, as is the case of the peak at 680 cm^{-1}. The reason for this apparently important change is due to the fact

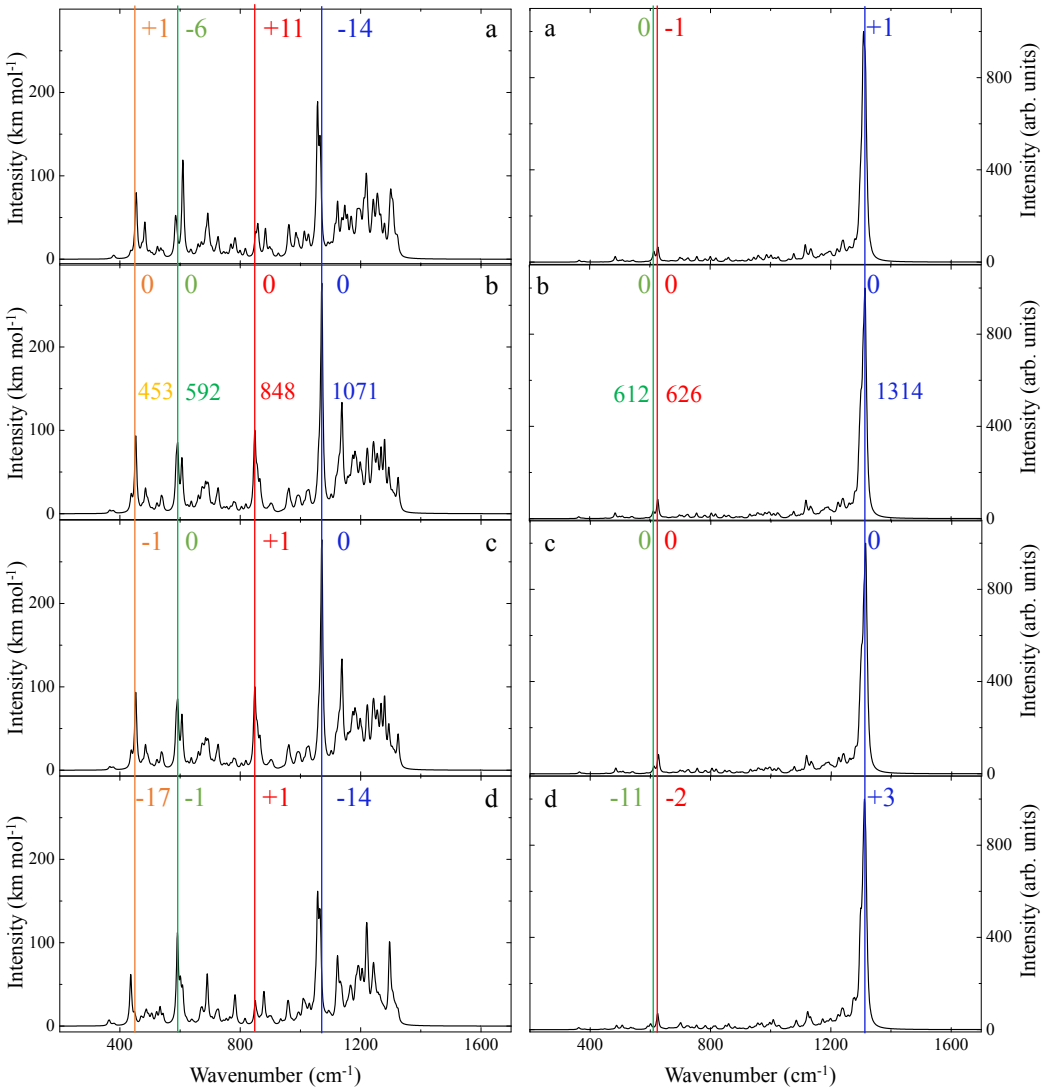

Figure 5: The IR (left) and Raman (right) spectra of the VN^- defect investigated with the DD model when the phosphorus atom is in position a, b, c and d (see figure 1-D). The vertical lines permit to appreciate the shift with respect to the b case.

that many wavenumbers *accumulate* in the same small spectroscopic region in some cases more than in others. Through the convolution process (8 cm^{-1} FWHM) they merge in a single peak, thus turning out to have a much higher intensity than in the cases in which the distance between the eigenvalues is slightly larger.

The Raman case (see Figure 5, right), with well separated peaks, permits an analysis that avoids the *superposition* problems just mentioned. The maximum shift is as small as 3 cm^{-1} for the peak at 1314 cm^{-1}, 2 cm^{-1} for the peak at 626 cm^{-1}, and increases to 11 cm^{-1} for the peak at 612 cm^{-1}, that seems the most sensitive to the P^+ position. These results, when compared with the IR ones just commented, seem to indicate that:

a) the low wavenumber peaks are the most sensitive to the P^+ position. However, the interaction produces a shift that is relatively small (11 cm^{-1}).

b) the medium shifts of the high wavenumber peaks in the IR spectrum seem to be due more to the problem of the correct identification of the peaks in the various cases (many peaks with the same symmetry do have very close wavenumbers) than to the real different interaction of the two defects when the P^+ position is changing.

It is clear that positions of the P^+ defect other than along the cube diagonal, would have permit to explore shorter distances between the defects, and lower symmetries. Both factors are obviously expected to increase the relative perturbation between the two defects.

Conclusions

In this study two different models for the simulation of charged defects in infinite systems (in the present case the VN^- defect in diamond) have been compared. The first one (CC), adopted systematically in the literature, consists in compensating with an uniform background of charge (positive in the present case) the extra charge, so as to obtain a neutral unit cell, a necessary condition for avoiding the "Coulomb catastrophe". This model is easily implemented, but not very physically grounded, because, for electrostatic reasons, in real

systems any negatively charged defect (say A) must have, at a relatively short distance, a compensating positively charged defect (say B).

In the second model another defect, of opposite charge (*double defect*, DD), is inserted; in this case the *auxiliary* defect is a P atom substituting a carbon. P transfers one electron to VN to give P^+ and VN^-. Obviously the influence of the B defect on the properties that usually are attributed to A depend on i) the extension of the perturbation generated by A, ii) the extension of the perturbation generated by B, iii) the A-B distance, and iv) the kind of property of interest. For a sufficiently large distance, the two defects can be considered independent. Exploring supercells containing 216, 512 and 1000 atoms, and various positions of the P^+ defect along the diagonal of the cube, it has been shown that, already with the smallest supercell:

a) the local geometry produced by CC and DD are extremely similar;

b) the same is true for the charge and spin distribution around the VN^- group;

c) also when delicate quantities depending on fine effects related to the spin density are compared, as the EPR constants, CC and DD perform in an extremely similar way;

d) the band structure are very similar, if the phosphorus energy levels are somehow excluded. The valence ones fall down in the valence bands, and are not visible. On the contrary, three P bands split from the *diamond* conduction bands by about 10mHa.

e) The P contribution appears, obviously, also in the vibrational spectrum (IR, in particular) Attributing to P a very large mass, it is possible to *eliminate* P from the IR and Raman spectra of DD, that appear then very close to the CC ones.

So, overall, and in spite of its *unphysical* nature, the CC model seems to perform as well as the DD one, at least when the *charge compensating defect* is not too close to the defect under investigation.

Some caution must be paid (see the subsection with title *is delocalized defect charge physically meaningful?* in Ref. 34), however, when LDA or GGA functionals are adopted in the simulation, as is the case for the near totality of the investigations performed in the past,

because in this case very often the local nature of the defect is lost and metallic solutions can be obtained, with spurious very long range effects.

Acknowledgements

FSG and AMF acknowledge the CINECA award (HP10BFOSPX) under the ISCRA initiative, for the availability of high performance computing resources and support.

References

(1) Dabo, I.; Kozinsky, B.; Singh-Miller, N. E.; Marzari, N. Electrostatics in Periodic Boundary Conditions and Real-Space Corrections. *Phys. Rev. B* **2008**, *77*, 115139.

(2) Freysoldt, C.; Neugebauer, J.; Van de Walle, C. G. Electrostatic Interactions between Charged Defects in Supercells. *Phys. Status Solidi B* **2011**, *248*, 1067–1076.

(3) Makov, G.; Payne, M. Periodic Boundary Conditions in Ab Initio Calculations. *Phys. Rev. B* **1995**, *51*, 4014.

(4) Lany, S.; Zunger, A. Assessment of Correction Methods for the Band-Gap Problem and for Finite-Size Effects in Supercell Defect Calculations: Case Studies for ZnO and GaAs. *Phys. Rev. B* **2008**, *78*, 235104.

(5) Sutherland, G. B. B. M.; Blackwell, D. E.; Simeral, W. G. The Problem of the Two Types of Diamond. *Nature* **1954**, *174*, 901–904.

(6) Davies, G. The A Nitrogen Aggregate in Diamond – its Symmetry and Possible Structure. *J. Phys. C* **1976**, *9*, L537–L542.

(7) Peaker, C. V.; Goss, J. P.; Briddon, P. R.; Horsfall, A. B.; Rayson, M. J. Di-Nitrogen–Vacancy–Hydrogen Defects in Diamond: a Computational Study. *Phys. Status Solidi A* **2015**, *212*, 2616–2620.

(8) Goss, J. P.; Briddon, P. R.; ; Papagiannidis, S.; Jones, R. Interstitial Nitrogen and its Complexes in Diamond. *Phys. Rev. B* **2004**, *70*, 235208.

(9) Mainwood, A. Modelling of Interstitial-Related Defects in Diamond. *Diamond Relat. Mater.* **1999**, *8*, 1560–1564.

(10) Kalish, R.; Reznik, A.; Prawer, S.; Saada, D.; Adler, J. Ion-Implantation-Induced Defects in Diamond and Their Annealing: Experiment and Simulation. *Phys. Status Solidi A* **1999**, *174*, 83–99.

(11) Davies, G.; Campbell, B.; Mainwood, A.; Newton, M.; Watkins, M.; Kanda, H.; Anthony, T. Interstitials, Vacancies and Impurities in Diamond. *Phys. Status Solidi A* **2001**, *186*, 187–198.

(12) Goss, J.; Jones, R.; Breuer, S.; Briddon, P.; Öberg, S. The Twelve-Line 1.682 eV Luminescence Center in Diamond and the Vacancy-Silicon Complex. *Phys. Rev. Lett.* **1996**, *77*, 3041.

(13) Gali, A.; Fyta, M.; Kaxiras, E. Ab Initio Supercell Calculations on Nitrogen-Vacancy Center in Diamond: Electronic Structure and Hyperfine Tensors. *Phys. Rev. B* **2008**, *77*, 155206.

(14) Siyushev, P.; Pinto, H.; Vörös, M.; Gali, A.; Jelezko, F.; Wrachtrup, J. Optically Controlled Switching of the Charge State of a Single Nitrogen-Vacancy Center in Diamond at Cryogenic Temperatures. *Phys. Rev. Lett.* **2013**, *110*, 167402.

(15) Dovesi, R. et al. Quantum-Mechanical Condensed Matter Simulations with CRYSTAL. *Wiley Interdisciplinary Reviews: Computational Molecular Science* **2018**, *8*, e1360.

(16) Dovesi, R. et al. CRYSTAL17 User's Manual; ; University of Torino, Torino, 2017.

(17) Becke, A. D. Density-Functional Thermochemistry. III. The Role of Exact Exchange. *J. Chem. Phys.* **1993**, *98*, 5648–5652.

(18) Lee, C.; Yang, W.; Parr, R. Development of the Colle-Salvetti Correlation-Energy Formula Into a Functional of the Electron Density. *Phys. Rev. B* **1988**, *37*, 785–789.

(19) Binkley, J. S.; Pople, J. A.; Hehre, W. J. Self-Consistent Molecular Orbital Methods. 21. Small Split-Valence Basis Sets for First-Row Elements. *J. Am. Chem. Soc.* **1980**, *102*, 939–947.

(20) Gentile, F.; Salustro, S.; Causá, M.; Erba, A.; Carbonniére, P.; Dovesi, R. The VN_3H Defect in Diamond. A Quantum Mechanical Investigation of the Structural, Electronic and Vibrational Properties. *Phys. Chem. Chem. Phys.* **2017**, *1*, 1–2.

(21) Gentile, F. S.; Salustro, S.; Di Palma, G.; Causà, M.; DâĂŹarco, P.; Dovesi, R. Hydrogen, Boron and Nitrogen Atoms in Diamond: a Quantum Mechanical Vibrational Analysis. *Theoretical Chemistry Accounts* **2018**, *137*, 154.

(22) Ferrari, A. M.; Salustro, S.; Gentile, F. S.; Mackrodt, W. C.; Dovesi, R. Substitutional Nitrogen Atom in Diamond. A Quantum Mechanical Investigation of the Electronic and Spectroscopic Properties. *Carbon* **2018**, *134*, 354–365.

(23) Salustro, S.; Gentile, F. S.; Erba, A.; Carbonniére, P.; El-Kelany, K. E.; Dovesi, R. The Characterization of the VNxHy Defects in Diamond through the Infrared Vibrational Spectrum. A Quantum Mechanical Investigation. *Carbon* **2018**, *132*, 210–219.

(24) Salustro, S.; Ferrari, A. M.; Gentile, F. S.; Desmarais, J. K.; Rérat, M.; Dovesi, R. Characterization of the B-Center Defect in Diamond through the Vibrational Spectrum: A Quantum-Mechanical Approach. *The Journal of Physical Chemistry A* **2018**, *122*, 594–600.

(25) Causà, M.; Dovesi, R.; Roetti, C. Pseudopotential Hartree-Fock Study of Seventeen III-V and IV-IV Semiconductors. *Phys. Rev. B* **1991**, *43*, 11937.

(26) Becke, A. D. A Multicenter Numerical Integration Scheme for Polyatomic Molecules. *J. Chem. Phys.* **1988**, *88*, 2547–2553.

(27) Pascale, F.; Zicovich-Wilson, C. M.; Gejo, F. L.; Civalleri, B.; Orlando, R.; Dovesi, R. The Calculation of the Vibrational Frequencies of the Crystalline Compounds and its Implementation in the CRYSTAL Code. *J. Comput. Chem.* **2004**, *25*, 888–897.

(28) Zicovich-Wilson, C. M.; Pascale, F.; Roetti, C.; Saunders, V. R.; Orlando, R.; Dovesi, R. Calculation of the Vibration Frequencies of α-Quartz: The Effect of Hamiltonian and Basis Set. *J. Comput. Chem.* **2004**, *25*, 1873–1881.

(29) Erba, A.; Ferrabone, M.; Orlando, R.; Dovesi, R. Accurate Dynamical Structure Factors from *Ab Initio* Lattice Dynamics: The case of Crystalline Silicon. *J. Comput. Chem.* **2013**, *34*, 346–354.

(30) Carteret, C.; De La Pierre, M.; Dossot, M.; Pascale, F.; Erba, A.; Dovesi, R. The Vibrational Spectrum of $CaCO_3$ Aragonite: a Combined Experimental and Quantum-Mechanical Investigation. *J. Chem. Phys.* **2013**, *138*, 014201.

(31) Baima, J.; Ferrabone, M.; Orlando, R.; Erba, A.; Dovesi, R. Thermodynamics and Phonon Dispersion of Pyrope and Grossular Silicate Garnets from *Ab Initio* Simulations. *Phys. Chem. Minerals* **2016**, *43*, 137–149.

(32) Pascale, F.; Zicovich-Wilson, C. M.; Orlando, R.; Roetti, C.; Ugliengo, P.; Dovesi, R. Vibration Frequencies of $Mg_3Al_2Si_3O_{12}$ Pyrope. An *Ab Initio* Study with the CRYSTAL Code. *J. Phys. Chem. B* **2005**, *109*, 6146–6152.

(33) Monkhorst, H. J.; Pack, J. D. Special Points for Brillouin-Zone Integrations. *Phys. Rev. B* **1976**, *13*, 5188.

(34) Komsa, H.-P.; Rantala, T. T.; Pasquarello, A. Finite-Size Supercell Correction Schemes for Charged Defect Calculations. *Phys. Rev. B* **2012**, *86*, 045112.